The tensile fracture behaviour of the aligned Al-Al_3Ni and Al-$CuAl_2$ eutectics at various temperatures

B. CANTOR*, G. J. MAY, G. A. CHADWICK†
Department of Metallurgy and Materials Science, University of Cambridge, UK

The tensile behaviour of single crystals of the unidirectionally-solidified Al-Al_3Ni fibrous and Al-$CuAl_2$ lamellar eutectics has been investigated at ambient and elevated temperatures. Fractured specimens have been studied directly by scanning electron microscopy, and longitudinal sections through each fracture surface by optical microscopy. At low temperatures, fracture of the Al-Al_3Ni eutectic is caused by the brittle failure of Al_3Ni fibres. At intermediate temperatures broken fibres may be present without causing composite fracture, whilst at high temperatures fibre pull-out occurs. The properties of the Al-$CuAl_2$ eutectic are controlled by the brittle $CuAl_2$ phase, except when the temperature is such that both phases are plastic. During fracture at high temperature the Al-$CuAl_2$ eutectic undergoes micromorphological degradation in the vicinity of the fracture surface.

1. Introduction

Unidirectionally-solidified eutectics have been studied because their strength coupled with good thermal stability may well give advantages over more conventional materials. The high temperature strength of a number of systems has been measured [1-5] but no work has been done specifically on the fractography of eutectic composites at varying temperatures. Salkind and co-workers [6, 7] have studied the tensile properties of aligned polycrystalline Al-Al_3Ni fibrous and Al-$CuAl_2$ lamellar eutectics up to 773 K (500° C). They found that the strength of both materials was reduced at elevated temperatures and that the Al-$CuAl_2$ eutectic began to show large elongations at temperatures greater than approximately 623 K (350° C). Crossman *et al* [8] confirmed these results for the Al-$CuAl_2$ eutectic, as did Butcher *et al* [9] who also observed microstructural coarsening after fracturing at high temperatures. Fractographic techniques have been used to study the room-temperature fracture of aligned polycrystalline Al-Al_3Ni eutectic in tension [6, 7, 10] and aligned polycrystalline Al-$CuAl_2$ eutectic in tension [6, 7, 10] and compression [11]. Tidy and Chadwick [12] have used scanning electron microscopy to study fracture surfaces of aligned single crystals of the Al-$CuAl_2$ eutectic deformed in bending at various temperatures.

The aim of the present work was to study the effect of temperature on the fracture characteristics of aligned single-crystal specimens of the Al-Al_3Ni eutectic and the Al-$CuAl_2$ eutectic. The fracture surfaces were studied by scanning electron microscopy and longitudinal sections were taken through the fracture surfaces and studied by optical microscopy.

2. Experimental procedure

Alloys of eutectic composition were made up from aluminium of 99.998% purity and copper and nickel of 99.999% purity. They were melted under argon in recrystallized alumina crucibles and cast into long flat ingots of rectangular cross-section. These ingots were placed singly in graphite moulds, enclosed in a silica tube, and directionally solidified horizontally under

*Now at the Applied Sciences Laboratory, University of Sussex, Falmer, Brighton, UK.
†Now at the Department of Mining and Metallurgical Engineering, University of Queensland, St Lucia, Brisbane, Australia.

argon in a travelling annular resistance furnace. The ingots were grown as single crystals by a "melt-back" technique [13] in which the solidification direction was reversed until a single grain resulted. The Al-Al_3Ni eutectic was grown at 110 mm h^{-1} and consisted of long Al_3Ni fibres of spacing 1.2 ± 0.2 μm; the Al-$CuAl_2$ eutectic was grown at 40 mm h^{-1} and had a lamellar spacing of 2.8 ± 0.3 μm. There were no bands of structural inhomogeneity in any of the crystals.

Tensile specimens were cut from the flat crystals by trepanning the gauge-length profile with a shaped tool on a spark machine. The gauge length, which was parallel to the growth direction, was typically 12.5 mm long and had a rectangular cross-section 3.5 by 3.0 mm. To remove surface damage, the Al-Al_3Ni eutectic was electropolished at 233 K (−40° C) and 15 V in an electrolyte of four parts methanol, one part perchloric acid; the Al-$CuAl_2$ eutectic was electropolished at 233 K and 12 V in a solution of one part concentrated nitric acid in nine parts methanol.

Tensile testing was carried out in air using an Instron testing machine with a furnace enclosing the specimen and grips. The system equilibrated at all temperatures within 30 min and tests were carried out as soon as the temperature had stabilized. After testing, the specimens had cooled to room temperature within 10 min. In the room-temperature tests the strain was measured directly with a Wiedemann-Baldwin microformer-type extensometer; in the high-temperature tests the strain was measured indirectly from the cross-head movement by making a correction for the machine compliance which was calculated from the room-temperature tests assuming that it was independent of temperature. In all tests the true strain-rate was 1.25 % per minute.

Specimens were prepared for optical metallography by grinding down to the finest grade of silicon carbide paper and polishing to 1 μm diamond compound. The Al-Al_3Ni specimens were then flash-electropolished under the conditions specified above and the Al-$CuAl_2$ eutectic was etched in warm dilute nitric acid. Fracture surfaces were examined directly with a "Stereoscan 2A" scanning electron microscope (SEM).

3. Results

3.1. Al-Al_3Ni eutectic

The stress-strain curves of the Al-Al_3Ni eutectic are shown in Fig. 1. At 293 K (20° C) and 593 K (320° C) the specimens exhibited no macroscopic plastic instability and at these temperatures failure occurred at stresses of 321 MNm^{-2} (33.2 kg mm^{-2}) and 123 MNm^{-2} (12.7 kg mm^{-2}) respectively. At 743 K (470° C) the system showed plastic instability at 81 MNm^{-2} (8.3

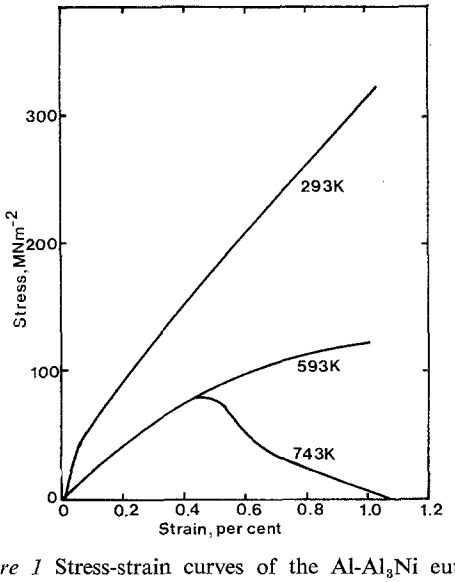

Figure 1 Stress-strain curves of the Al-Al_3Ni eutectic tested in tension at several temperatures.

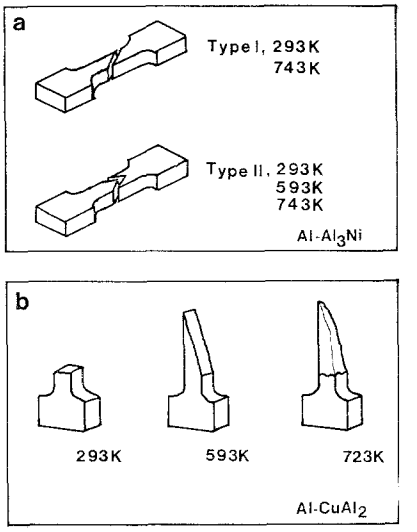

Figure 2 Schematic macroscopic appearance of specimens fractured at several temperatures (a) Al-Al_3Ni (b) Al-$CuAl_2$.

kg mm^{-2}) after which the stress decreased gradually to zero. At all temperatures the strain to failure was approximately 1% and failure always occurred within the gauge length.

The macroscopic appearance of fractured specimens is illustrated schematically in Fig. 2. The fracture surface was at an angle of 45° to the tensile axis in all cases. Irrespective of testing temperature, specimens which showed type I behaviour were striation-free (contained no low angle sub-boundaries), whilst those which exhibited type II behaviour had a striation sub-boundary at the apex of the two parts of the fracture surface.

Optical micrographs of longitudinal sections through the fracture surface of specimens tested at 293 K showed that there were a few fibre-breaks close to the fracture surface but none elsewhere. Specimens with type II behaviour displayed no greater frequency of fibre fracture at the apex. Elongated dimples of aluminium (Fig. 3), which were formed as the ductile aluminium necked around broken Al_3Ni fibres, were observed on the fracture surface in the SEM. Fig. 3 also shows similar behaviour behind the main fracture surface in the region indicated by an arrow.

At 593 K there were more broken fibres throughout the specimen, some being localized in bands close to the fracture surface as shown in Fig. 4. The fracture surface (Fig. 5), characteristically consisted of long narrow regions of elongated dimples separated by extensive walls where shear had taken place in the matrix. The height of the shear walls, approximately 20 μm, corresponded with the length of many of the pre-cracked fibre segments, as can be seen by comparing Figs. 4 and 5. A specimen loaded to 0.8% strain at 593 K and then unloaded

Figure 3 Scanning electron micrograph of the fracture surface of Al-Al_3Ni eutectic tested at 293 K showing elongated dimples and fibre breaks (arrowed) behind the main fracture surface (× 800).

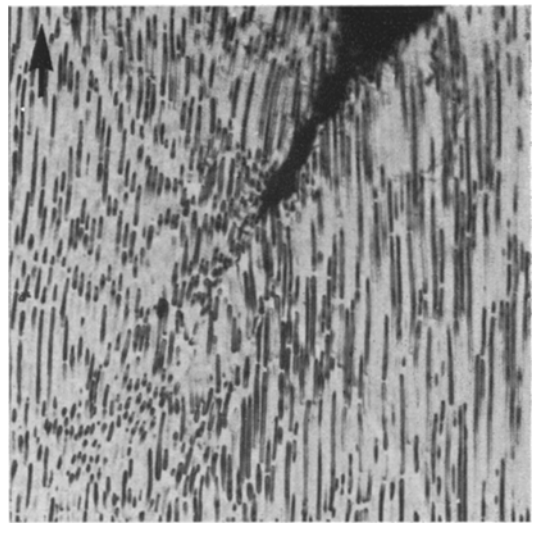

Figure 4 Optical micrograph of Al-Al_3Ni eutectic tested at 593 K showing bands of broken fibres. Al_3Ni phase etched black. The arrow denotes the stress axis (× 750).

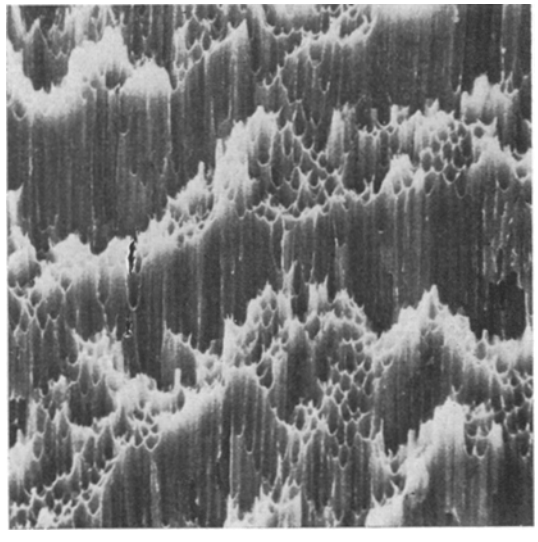

Figure 5 Scanning electron micrograph of the fracture surface of Al-Al_3Ni eutectic tested at 593 K showing walls of shear in the matrix between rows of fibres (× 900).

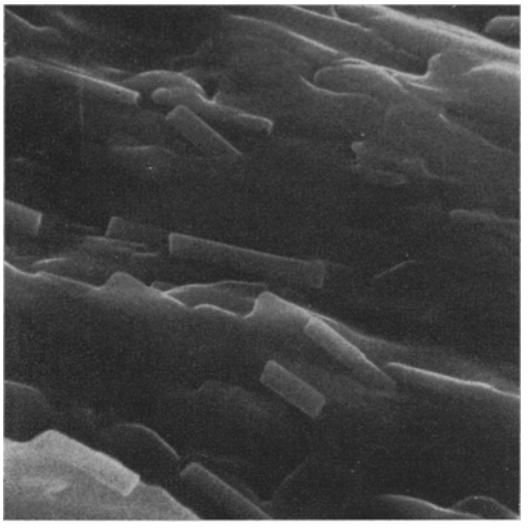

Figure 6 Scanning electron micrograph of the fracture surface of Al-Al_3Ni eutectic tested at 743 K showing pulled out fibres lying on the surface (× 4500).

contained practically no broken fibres.

Lying on the fracture surface at 743 K were pulled-out fibres which were approximately 5 μm in length and had square ends characteristic of brittle failure (Fig. 6). Optical micrographs showed that there were fewer fibre fractures at 743 K than at 593 K.

3.2. Al-$CuAl_2$ eutectic

The stress-strain curves of the Al-$CuAl_2$ eutectic are shown in Fig. 7. At 293 K the specimens showed no plastic instability and failed at a stress of 276 MNm^{-2} (28.5 kg mm^{-2}) and a strain of 0.87%. At higher temperatures the strength fell off rapidly, plastic instability was exhibited, and the specimens subsequently failed with the stress gradually diminishing to zero. The UTS at 593 K was 157 MNm^{-2} (16.2 kg mm^{-2}) and the failure strain 4.1%; at 723 K (450° C) the UTS was 43 MNm^{-2} (4.7 kg mm^{-2}) and the strain to failure was 4.9%. The Al-$CuAl_2$ specimens all failed within the gauge length.

The macroscopic appearance of fractured specimens is shown schematically in Fig. 2,

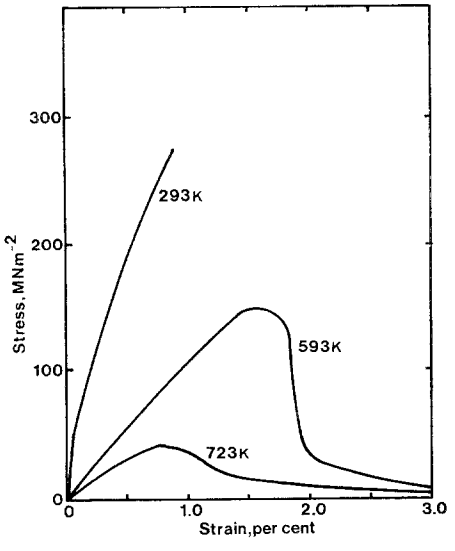

Figure 7 Stress-strain curves of the Al-$CuAl_2$ eutectic tested at several temperatures.

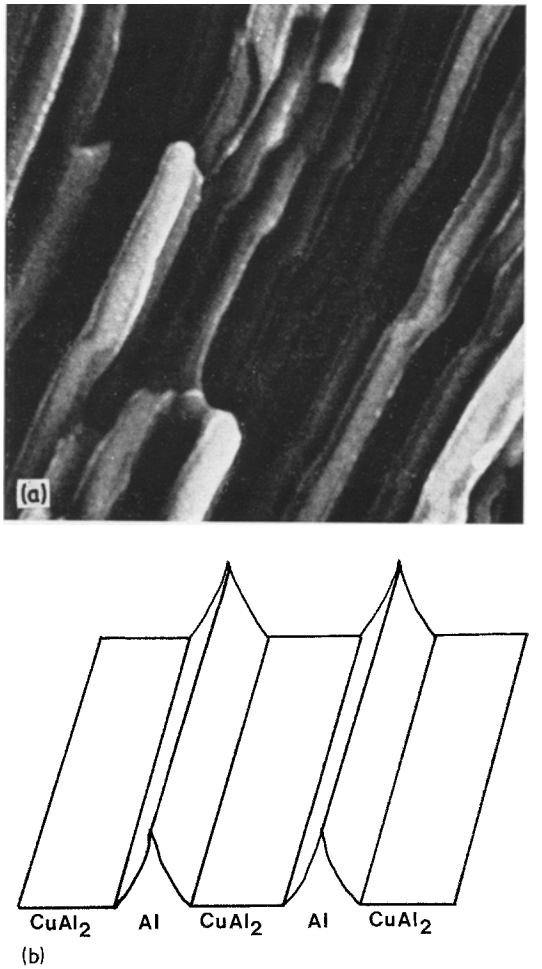

Figure 8 (a) Scanning electron micrograph of the fracture surface of Al-$CuAl_2$ eutectic tested at 293 K showing ductile failure of Al lamellae between brittle fractured $CuAl_2$ lamellae (× 3200). (b) Schematic diagram showing distribution of phases in Fig. 8a.

which illustrates the effect on the fracture characteristics of the change from brittle behaviour of the $CuAl_2$ phase at room temperature to increasingly ductile behaviour at higher temperatures. The fracture path changes from being transverse to being at a small angle to the tensile axis as the temperature is raised.

At 293K the microscopic appearance of the fracture surface showed planar surfaces of $CuAl_2$ which had failed in a brittle fashion, alternating with ridged profiles of the aluminium phase drawn out to an edge by ductile tearing (Fig. 8). Optical micrographs showed that behind, but close to the fracture surface, there were broken lamellae of the $CuAl_2$ phase.

At 593K the fracture surface as observed in the SEM consisted mainly of platelets exposed during crack propagation by shear in the aluminium phase (Fig. 9). Optical micrographs showed that the $CuAl_2$ lamellae were bent and broken (Fig. 10). Voids were observed close to the fracture surface along interphase boundaries and were accommodated by distortion of the lamellae. These features were demonstrated to be voids by polishing to successive levels and thus observing the features three-dimensionally.

In the Al-$CuAl_2$ eutectic tested at 723K the fracture surface consisted mainly of regions of small rounded protrusions (Fig. 11), but other regions consisted of fragmented $CuAl_2$ lamellae exposed by shear in the matrix. Degradation of the original lamellar micromorphology had occurred in a zone of approximately 0.3 mm from the fracture surface (Fig. 12a), yielding an equiaxed structure, the scale of which correlated with the protrusions on the fracture surface. Longitudinal voids were also observed in the microstructure, as shown in Fig. 12b.

To examine the fracture mechanism at 723K a specimen which had a small transverse notch spark-machined in its gauge length was tested in tension to just beyond the UTS. The crack propagated by the coalescence of large voids

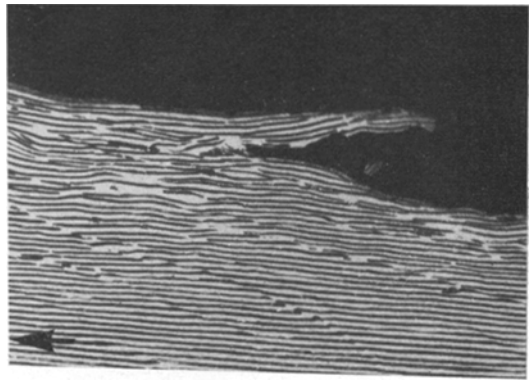

Figure 10 Optical micrograph of Al-$CuAl_2$ eutectic tested at 593K showing crack propagation along lamellae and some small voids. $CuAl_2$ phase etched black. The arrow denotes the stress axis (× 250).

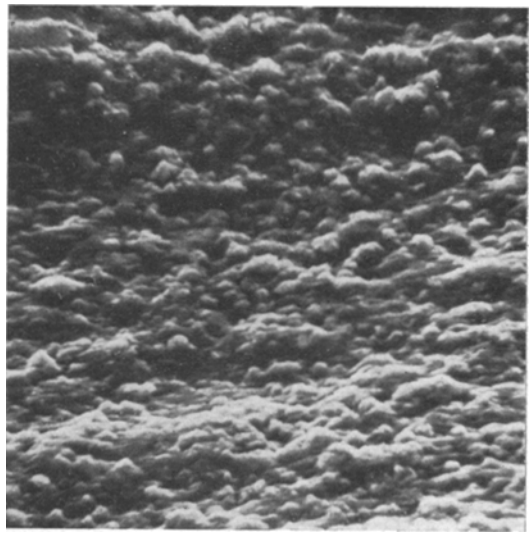

Figure 11 Scanning electron micrograph of the fracture surface of Al-$CuAl_2$ eutectic tested at 723K showing coarsened microstructure (× 900).

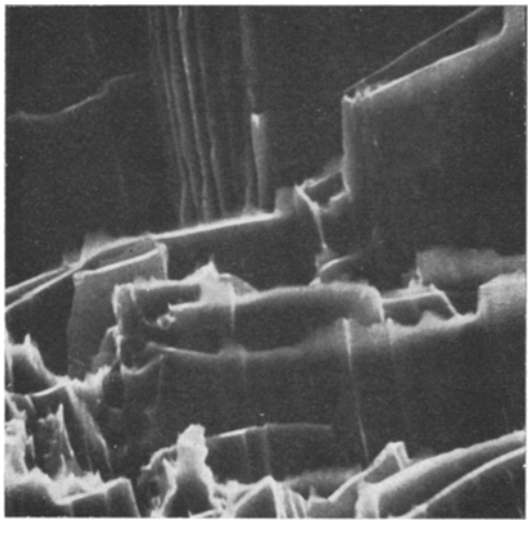

Figure 9 Scanning electron micrograph of the fracture surface of Al-$CuAl_2$ eutectic tested at 593K showing lamellae exposed by shear (× 900).

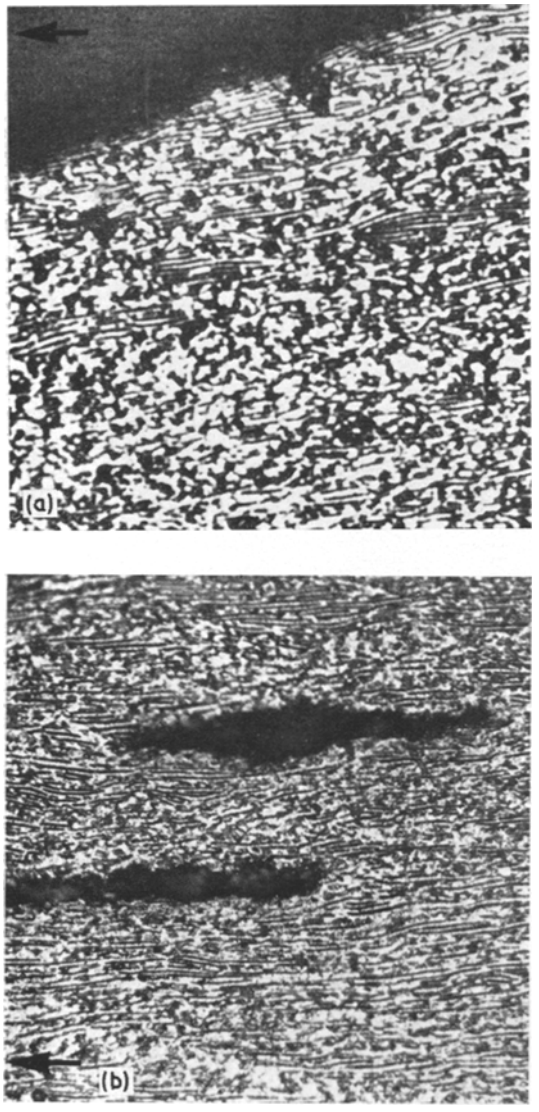

Figure 12 Optical micrographs of Al-$CuAl_2$ eutectic tested at 723K showing (a) coarsened microstructure (× 315); (b) voids behind the fracture surface approximately parallel to lamellae (× 340). $CuAl_2$ phase etched black. The arrows denote the stress axis.

which had opened up along lamellar interfaces (Fig. 13). The fracture surface had an undulating appearance as would be expected from a void-coalescence crack-growth mechanism. The structure had not degenerated in the region of the stress concentration around the root of the notch but degradation of lamellae had begun where the crack had started to propagate. Similar specimens which were tested to stresses below the UTS did not exhibit micromorphological degradation.

4. Discussion

The fracture resistance of Al-Al_3Ni eutectic tested at 293K is controlled by the brittle failure of Al_3Ni fibres. Shortly before the composite fails all the fibres are close to their failure strain. Detection of fibre-cracking by optical microscopy and acoustic emission [14] shows that very few fibres are cracked prior to composite failure. Consequently, a small number of fibre breaks rapidly leads to composite failure, because of the stress concentration in regions close to them. The ductile aluminium matrix necks around broken fibres, forming a dimpled fracture surface.

Fibre-reinforced composites conventionally fracture transverse to the tensile axis [15] and this has been reported for aligned Fe-Fe_2B eutectic [1]. In all cases, the fracture surfaces in Al-Al_3Ni eutectic are at 45° to the tensile axis and similar behaviour has been observed in aligned Cu-Cr eutectic [16] and pearlite [17].

This difference in fracture behaviour may be related to the stress-transfer mechanism in the matrix close to fibre breaks. When local stresses due to a fibre break are transmitted elastically by the matrix, the maximum stress concentration on an adjacent fibre is at 90° to the tensile axis. Adjacent fibres fracture in this plane and when fibre breaks are linked by ductile failure of the matrix, the macroscopic fracture surface is also at 90° to the tensile axis (Fig. 14a). Alternatively, local stresses may be transmitted by matrix shear. The maximum stress concentration on adjacent fibres is then along a plane at 45° to the tensile axis from the initial break, and the macroscopic fracture surface is also in this plane (Fig. 14b).

For a ductile matrix, elastic stress transfer would be expected to predominate when the matrix is inhibited from deforming plastically by the presence of closely spaced fibres. Although the exact nature of this type of matrix constraint is not yet clear [1, 18-20], the effect will be smaller for low-volume fraction composites and for large interfibre spacings. Thus in Al-Al_3Ni, Cu-Cr and pearlite, with low-volume fraction reinforcement, matrix shear produces 45° fracture surfaces; in Fe-Fe_2B and most conventional composites, the high-volume fraction reinforcement inhibits matrix shear and produces transverse fracture surfaces. Stress transfer by matrix

Figure 13 Optical micrograph of notched specimen of Al-$CuAl_2$ eutectic tested at 723 K showing initial crack propagation by void coalescence. $CuAl_2$ phase etched black. The arrow denotes the stress axis (× 560).

shear also explains why dimples on the fracture surfaces of Al-Al_3Ni are elongated along the 45° plane (Fig. 14b). In previous models [6, 16] this has only been explained on the assumption that fibres are discontinuous, although Al_3Ni fibres have been shown to have aspect ratios of at least 10000:1 [10].

At 593 K the matrix constraint in Al-Al_3Ni is reduced and the transition from elastic fibres/elastic matrix to elastic fibres/plastic matrix is not observed. At this temperature, the composite is able to contain a greater concentration of pre-cracked fibres without failing than at 293 K. This is because the aluminium matrix is more ductile and more able to remove stress concentrations by plastic flow. The effect of these pre-cracked fibres on the fracture behaviour is shown in Fig. 14c. A crack advances along a plane of maximum matrix shear and periodically links with pre-cracked fibres, creating the shear walls observed in the SEM.

At 743 K, Al_3Ni fibres are pulled out of the matrix during fracture. The stress σ_e to extract a fibre of embedded length x and diameter d, is given by:

$$\sigma_e = \sigma_0 + k_1 x/d$$

where k_1 and σ_0 are constants [21]. If the fibre end is not attached to the matrix σ_0 is zero. Fibre pull-out is resisted by the shear strength both of the matrix and fibre/matrix interface. If deformation results solely from pull-out, the composite strain is given by:

$$\epsilon \propto -x .$$

Thus the stress on the composite is inversely proportional to the strain:

$$\sigma = \sigma_0 - k_2 \epsilon$$

where k_2 is a constant. Fig. 1 shows that from just beyond the UTS (about 0.7% strain), the stress-strain curve of Al-Al_3Ni is approximately linear with negative slope. Thus deformation beyond the UTS is predominantly by pull-out with the stress gradually decreasing to zero. Pull-out may occur as the temperature is increased due to a decrease in either the matrix shear strength or the fibre/matrix interface shear strength.

At 293 K failure of aligned Al-$CuAl_2$ eutectic is caused by a few brittle fractures of the $CuAl_2$ phase and the aluminium fails in a ductile manner

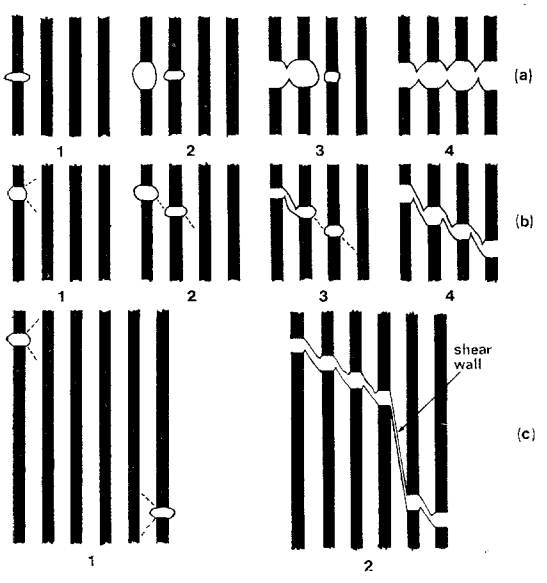

Figure 14 Diagram of fracture modes in aligned composites. In (a) elastic stress concentration around a fibre break causes fracture of adjacent fibres and composite failure at 90° to the tensile axis. In (b) shear in the matrix causes fracture of adjacent fibres and composite failure at 45° to the tensile axis. In (c) the presence of pre-cracked fibres causes shear walls in the matrix during composite failure.

between cracked $CuAl_2$ lamellae. Although the fracture surfaces are always at an angle of 90° to the tensile axis and the volume fraction is close to 50%, it cannot be assumed that the fracture mechanism is that shown in Fig. 14a. Adjacent $CuAl_2$ lamellae are continuous at lamellar faults and a crack can travel throughout this phase without local stress propagation through the matrix [12].

At 593K both phases are ductile and the stress-strain curve shows plastic instability. A crack is initiated by the formation of voids along interphase boundaries. The voids grow and coalesce, giving an undulating appearance to this region of the fracture surface. The crack continues to propagate by microscopic shear, exposing lamellae on the fracture surface. Most of this crack propagation is parallel to the lamellae, and the resulting fracture surface is at a small angle to the tensile axis.

At 723K cracks are initiated in a manner similar to that at 593K. Subsequent crack growth occurs by ductile tearing in regions of micromorphological degradation. Degradation is only observed after the crack has started to propagate. Thus, micromorphological degradation is the result of severe local deformation and fragmentation at the crack tip during propagation, and not caused by deformation prior to crack initiation.

At 723K the observed failure strain in the Al-$CuAl_2$ eutectic is much lower than that reported by other workers who have observed a superplastic type of behaviour at high temperatures. Butcher *et al* [9] state that their tests were carried out at strain-rates of 5 to 6% min^{-1} while Crossman *et al* [8] quote a nominal strain of 1% min^{-1}. In the present experiments the true strain-rate was 1.23% min^{-1} but the machine cross-head strain-rate was 39.4% min^{-1}. Since superplasticity is a thermally activated process it is sensitive to strain-rate: it is therefore concluded that the absence of superplastic behaviour results from the tests being carried out at a relatively high strain-rate, and that the strain-rates quoted by previous workers are nominal rather than true strain-rates.

5. Conclusions

The aligned Al-Al_3Ni eutectic fractures by three different mechanisms at 293, 593, and 743K. At the lowest temperature local stresses around the first few fibre-breaks are transferred to adjacent fibres by matrix shear and failure rapidly takes place along a fracture plane at 45° to the tensile axis. This is different from conventional failure modes, in which elastic stress transfer is sufficient to fracture adjacent fibres, and fracture occurs at 90° to the tensile axis. At 593K the fracture mechanism is similar to that at 293K but the presence at the fracture point of a greater concentration of pre-cracked fibres produces shear walls in the matrix. At the highest temperature, 743K, fracture propagation is by fibre pull-out, probably due to either increased matrix ductility or weaker interfacial bonding. At all testing temperatures fracture is initiated at striation subboundaries if these are present.

The aligned Al-$CuAl_2$ eutectic fractures by three different mechanisms at 293, 593,and 723K. At the lowest temperature the first lamellar breaks rapidly lead to failure because the $CuAl_2$ phase is continuous. At 593 and 723K fracture is initiated by the appearance of voids in the microstructure in planes parallel with the lamellae. At 593K the voids link up by shear deformation of both phases in the lamellar plane. However, at 723K, the voids are linked by ductile tearing of the two phases. At this tem-

perature, morphological degradation occurs concurrent with ductile tearing and leads to a local microduplex region at the fracture surface.

Acknowledgements

B. Cantor wishes to thank the Science Research Council for the tenure of an SRC studentship. G. J. May gratefully acknowledges the financial support of the Ministry of Defence (Procurement Executive).

References

1. A. R. T. DE SILVA and G. A. CHADWICK, *Met. Sci. J.* **3** (1969) 168.
2. J. L. WALTER and H. E. CLINE, *Met Trans.* **1** (1970) 1221.
3. H. E. CLINE, *Trans. AIME* **239** (1967) 1906.
4. YUAN-SHOU SHEN and L. B. GRIFFITHS, *Met. Trans.* **1** (1970) 2305.
5. E. R. THOMPSON, D. A. KOSS, and J. C. CHESNUTT, *Met Trans.* **1** (1970) 2807.
6. M. J. SALKIND, F. D. LEMKEY, and F. D. GEORGE, 'Whisker Technology" (J. Wiley, New York, 1967).
7. M. J. SALKIND, B. J. BAYLES, F. D. GEORGE, and W. K. TICE (United Aircraft Corp.) Final Rep. Contract No. NOW64-0433-d, (1965).
8. F. W. CROSSMAN, A. S. YUE, and A. E. VIDOZ, *Trans AIME* **245** (1969) 397.
9. B. R. BUTCHER, G. C. WEATHERLEY, and H. R. PETTIT, *Met. Sci. J.* **3** (1967) 7.
10. R. W. HERTZBERG, F. D. LEMKEY, and J. A. FORD, *Trans. AIME* **233** (1965) 342.
11. A. PATTNAIK and A. LAWLEY, *Met. Trans.* **2** (1971) 1529.
12. D. C. TIDY and G. A. CHADWICK, to be published.
13. G. A. CHADWICK, *Progr. Mater. Sci.* **12** (1963) 97.
14. D. O. HARRIS, A. S. TETELMAN, and F. A. I. DARWISH, Tech. Rep. No. DRC-71-1, Dunegan Research Corp. (1971).
15. See for example A. KELLY and G. J. DAVIES, *Met. Rev.* **10** (1965) 1.
16. R. W. HERTZBERG and R. W. KRAFT, *Trans. AIME* **227** (1963) 580.
17. L. E. MILLER and G. C. SMITH, *JISI* **208** (1970) 998.
18. A. KELLY and H. LILHOLT, *Phil. Mag.* **20** (1969) 311.
19. P. NEUMAN and P. HAASEN, *ibid.* **23** (1971) 285.
20. B. CANTOR, Ph.D thesis, University of Cambridge (1972).
21. A. KELLY, *Proc. Roy. Soc. Lond.* **319A** (1970) 95.

Received 20 July and accepted 20 November 1972.